Article ID: 1000-7032(2026)05-0725-11

Pressure-responsive Fluorescent Behavior and Sensing Performance of Anthracene/Montmorillonite Composites

ZHANG Guangqing[1], SU Ke[1], LIU Zunqi[2], LIAO Libing[1], MEI Lefu[1,2*]

(1. *Engineering Research Center of Ministry of Education for Geological Carbon Storage and Low Carbon Utilization of Resources, Beijing Key Laboratory of Materials Utilization of Nonmetallic Minerals and Solid Wastes, National Laboratory of Mineral Materials, School of Materials Science and Technology, China University of Geosciences (Beijing), Beijing* 100083, *China*;
2. *Chemistry and Chemical Engineering College, Xinjiang Agricultural University, Urumqi* 830052, *China*)
* *Corresponding Author, E-mail: mlf@cugb. edu. cn*

Abstract: Visualization-enabled monitoring under extreme pressure requires luminescent systems that can directly convert pressure variations into a readable and quantifiable spectral shift or color change. Organic luminophores are intrinsically sensitive to molecular packing and the local microenvironment, offering strong potential for pressure-induced color tuning, yet their high-pressure applications are often limited by solid-state aggregation-caused quenching and insufficient stability. Here, anthracene (An) was employed as the emissive unit and confined *via* an interlayer-intercalation strategy within organo-modified montmorillonite to form An-based composites. As the intercalation ratio increases from 2∶1 to 1∶12, the (001) reflection continuously shifts to lower angles with an expanded basal spacing, indicating effective intercalation and homogeneous dispersion of An, accompanied by a pronounced enhancement in solid-state emission; the confined and hydrophobic interlayer environment further prolongs the emission lifetime. *In situ* diamond anvil cell measurements show that the 1∶12 composite exhibits a continuous red shift of the emission maximum with a visible color evolution from bluish-violet to yellow upon compression. A strong linear relationship between peak position and pressure is obtained over 1. 60−10. 1 GPa (R^2=0. 996), with partial reversibility during decompression. These results demonstrate that interlayer confinement can simultaneously unlock the piezochromic advantages of organic emitters while suppressing solid-state quenching, providing an effective route toward visualization-enabled fluorescent manometry materials.

Keywords: anthracene; organic-inorganic composite materials; pressure sensing
CLC number: O482. 31 **Document code**: A
DOI: 10. 37188/CJL. 20260002 **CSTR**: 32170. 14. CJL. 20260002

蒽/蒙脱石复合材料的压力响应荧光行为及传感性能

张光晴[1], 苏 科[1], 刘尊奇[2], 廖立兵[1], 梅乐夫[1,2*]

(1. 中国地质大学(北京) 材料科学与工程学院, 矿物材料国家专业实验室,
非金属矿物与固废资源材料化利用北京市重点实验室, 地质碳储与资源低碳利用教育部工程研究中心, 北京 100083;
2. 新疆农业大学 化学与化学工程学院, 新疆 乌鲁木齐 830052)

摘要: 极端压力环境下的可视化监测需要将外压变化直接转化为可读、可定量的光谱位移或颜色变化。有机发光分子对分子堆积与微环境极其敏感,因而天然具备“压力诱导变色”的高响应潜力,但其固态聚集猝灭与稳定性不足限制了高压应用。为此,本工作以蒽(An)为发光单元,采用插层限域策略将其引入有机改性蒙脱石层间构筑复合材料。随着插层比例由 2∶1 提升至 1∶12,(001)衍射峰持续向低角度移动且层间距逐步增大,

收稿日期: 2026-01-03; **修订日期**: 2026-01-12
基金项目: 国家自然科学基金(52274273)
Supported by National Natural Science Foundation of China (52274273)

表明蒽实现有效插层与均匀分散，并显著增强固态发光；限域与疏水微环境进一步延长了发光寿命。金刚石对顶砧原位变压测试显示，1∶12样品随压力升高发射峰规律红移，发光颜色由蓝紫连续转变为黄光；在1.60~10.1 GPa范围内，峰位与压力呈良好线性关系（R^2=0.996），且卸压具有一定可逆性。该结果证明，插层限域可同时释放有机分子的压致变色优势并抑制固态猝灭，为可视化荧光测压材料提供了有效路径。

关 键 词：蒽；有机-无机复合材料；压力传感

1 Introduction

Piezochromic materials represent a class of smart materials responsive to mechanical stimuli, exhibiting high sensitivity to external environments[1-2]. By changing the molecular packing arrangements under applied mechanical stress, these materials alter their emission colors and intensities, making them highly promising in various applications such as pressure sensors, information storage, anti-counterfeiting, and optoelectronic devices[3-5]. Achieving precise and tunable modulation of emission and absorption spectra over a broad pressure range is critical for enhancing the functionality of piezochromic materials[6-7]. Pressure is a thermodynamic parameter independent of temperature and composition, capable of significantly altering molecular structures and properties. With rapid advances in *in-situ* structural and property measurement technologies under high pressures, pressure has increasingly become a crucial tool in scientific research. Recently, high-pressure techniques have been introduced into the field of piezochromic materials as a form of mechanochemistry. High pressure can effectively shorten intermolecular distances, thereby modifying molecular packing more efficiently and precisely controlling the emission color and intensity[8-9].

Pressure can directly influence molecular conformation and aggregation structures, thereby inducing transformations in photophysical properties of materials[3,10-11]. Under high-pressure conditions, intermolecular and interatomic distances within organic molecular aggregates can be significantly reduced, enhancing molecular aggregation and modifying molecular geometries (such as distances and angles). This process alters electron cloud overlap densities and rearranges molecular orbital configurations[12], consequently destabilizing the system and triggering notable changes in crystal structures, molecular structures, and electronic structures[13]. Such structural transformations ultimately affect the electronic transport and optical properties of the materials. The application of pressure-induced luminescence color changes (piezochromism) in organic materials and their exploration in pressure-sensing applications remain at an early stage. Therefore, the development of smart luminescent materials capable of sensitively detecting pressure variations is of great significance[14-17].

Anthracene, as a typical wide-bandgap polycyclic aromatic hydrocarbon (PAH), is often chosen as a representative model by researchers to investigate and extrapolate the properties of other more structurally complex PAHs[18]. Thus, anthracene and its derivatives frequently serve as model compounds for exploring the impact of high-pressure conditions on organic luminescent materials[19]. Anthracene, an organic molecule consisting of three fused benzene rings with the molecular formula $C_{14}H_{10}$, exhibits strong and stable blue-violet fluorescence under ultraviolet illumination at ambient conditions[20]. The extensive conjugated π-system within anthracene facilitates efficient $\pi \rightarrow \pi^*$ transitions under ultraviolet excitation, accompanied by significant energy absorption. Additionally, its rigid molecular framework reduces non-radiative energy loss due to molecular vibrations, thus endowing anthracene with excellent luminescent properties. To date, anthracene has shown promising potential in various fields such as biological fluorescent probes, scintillators, electroluminescent devices, and solar cells. Nevertheless, pure organic luminescent materials often suffer from aggregation-induced spectral shifts, broadening, or fluorescence quenching, substantially reducing their

emission efficiencies in practical device applications[21-24].

Montmorillonite is a typical natural mineral with a nanoscale layered structure[25]. Due to isomorphic substitutions such as the replacement of Al^{3+} in octahedral sheets by Mg^{2+} or Fe^{2+}, or the substitution of Si^{4+} in tetrahedral sheets by Al^{3+} or Fe^{3+}—excess negative charges are generated within its layers[26]. These negative charges are balanced by the electrostatic adsorption of interlayer cations such as K^+, Na^+, Ca^{2+}, and Mg^{2+}, resulting in electrical neutrality of the crystal structure. Montmorillonite exhibits excellent swelling, adsorption, and cation-exchange capacities. Owing to its abundant availability and low cost, montmorillonite is extensively employed in the fabrication of polymer-layered silicate nanocomposites. Moreover, the unique properties of its interlayer domain provide favorable conditions for synthesizing inorganic-organic functional materials[27-28]. By adjusting the layer charges, one can precisely modify the micro-electric field environment within the interlayer regions and thus control the interactions with interlayer cations. Consequently, it becomes possible to finely tune the properties of inorganic-organic composite materials, enabling the design of functional inorganic-organic composites with continuously adjustable properties[29-30].

In this study, anthracene molecules were intercalated into organically modified montmorillonite (m-MMT) interlayers. The resulting anthracene/m-MMT composites exhibited significantly enhanced fluorescence intensity compared to pure anthracene. This improvement arises from the uniform dispersion of anthracene within the m-MMT interlayers, effectively mitigating concentration-induced quenching and leading to enhanced luminescence. Additionally, the fluorescence lifetime of the composite materials was notably prolonged compared to pure anthracene. Upon applying high pressure, the synthesized anthracene/m-MMT composites demonstrated remarkable piezochromic characteristics, with the fluorescence color gradually shifting from bluish-violet to yellow as external pressure increased. Further investigations of the luminescent and pressure-sensing properties of the composites revealed excellent linear correlations between the fluorescence emission wavelength and intensity changes within the pressure range of 1.60−10.1 GPa. The experimental wavelengths closely matched the fitted linear regression curves, with a fitting coefficient of 0.996. This monotonic change with applied pressure provides a novel approach for developing luminescent pressure sensors suitable for extreme environmental conditions.

2　Experiment

2.1　Materials

The calcium-based montmorillonite was sourced from Ningcheng City, Inner Mongolia, and had a cation exchange capacity (CEC) of 90 mmol/100 g. The other chemicals were used as received: anthracene ($C_{14}H_{10}$, 99%) and cetyltrimethylammonium bromide (CTAB, 99%), both purchased from Macklin Biochemical Technology Co., Ltd. (Shanghai, China).

2.2　Preparation of Organically Modified Montmorillonite

A total of 5 g of montmorillonite (MMT) was placed in a 1 L beaker with 500 mL of deionized water and stirred magnetically for 1 h to allow complete swelling and to obtain a uniform dispersion. Subsequently, an amount of hexadecyl trimethyl ammonium bromide (CTAB), an organic modifier used to enhance the hydrophobicity and expand the interlayer spacing of the clay, equivalent to 1 CEC was added to the dispersion and stirred for 4 h. The mixture was centrifuged at 10 000 r/min to separate the solids, and the supernatant was discarded. The residue was washed with deionized water three times and then dried in an oven at 60 ℃ for 12 h. The dried material was ground and sieved through a 200-mesh sieve.

2.3　Intercalation of Anthracene into Organically Modified MMT

A specified amount of anthracene was dissolved in 50 mL of acetone in a 100 mL beaker by stirring until completely dissolved. Separately, 0.2 g of organically modified MMT was dispersed in 50 mL of

deionized water in a 200 mL beaker and stirred magnetically for 30 min. The anthracene solution was then added to the MMT dispersion, and the mixture was stirred under dark conditions for 15 h. The resulting material was centrifuged at 10 000 r/min, and the supernatant was discarded. The residue was washed four times with deionized water, dried at 60 ℃ for 12 h, and ground into a fine powder. Composites were prepared by adding anthracene to the organically modified MMT at different loadings, corresponding to nominal molar ratios of the pre-intercalated CTAB to the added anthracene (CTAB∶An) of 2∶1, 1∶1, 1∶2, 1∶3, 1∶4, 1∶6, 1∶8 and 1∶12.

2.4 Characterization

X-ray diffraction (XRD) was performed using a Bruker D8 Advance Diffractometer to analyze the crystal structure. Fourier transform infrared spectroscopy (FTIR) spectra were recorded using a Spectrum 100 Spectrometer in the range of 4 000–400 cm^{-1}. Scanning electron microscopy (SEM) images were obtained with a JSM-7601F (JEOL, Japan) to study the morphology. Fluorescence excitation and emission spectra at room temperature were measured using a Hitachi F-4700 Fluorescence Spectrophotometer. Thermal stability was assessed by thermogravimetric analysis (TGA) using a TG/DTA 6300 Analyzer (Hitachi, Japan) in a nitrogen atmosphere with a temperature range of room temperature to 600 ℃ at a heating rate of 10 ℃/min. High-pressure experiments employed a symmetric diamond anvil cell (DAC) to measure variable-pressure spectra using a 355 nm laser excitation source and an Ocean Optics QE6500 Fiber Optic Spectrometer, with images captured by a digital camera.

3 Results and Discussion

3.1 Structural and Micromorphology of Anthracene/Organic Montmorillonite Composites

The calcium-based montmorillonite was organically modified using CTAB. After CTAB entered the interlayer of montmorillonite, it created a hydrophobic environment between the layers. By intercalating anthracene into organically modified montmorillonite at controlled molar ratios of CTAB to anthracene ranging from 2∶1 to 1∶12, a series of composites with progressively increasing anthracene content were prepared (Fig. 1(a)). Structural characterization and performance tests were performed on these composites. To investigate whether anthracene entered the organic montmorillonite layers, XRD patterns of anthracene, organic montmorillonite (m-MMT), and the composites were obtained, with the test results shown in Fig. 1(b). By comparing the XRD diffraction peaks of the composites with those of organic montmorillonite, it was observed that when the intercalated anthracene concentration was 1∶1, the diffraction peak corresponding to the (001) crystal plane of montmorillonite did not appear prominently in the composite (Fig. 1(c)). Based on previous studies[31], a reasonable explanation for this phenomenon is that the low concentration of anthracene resulted in insufficient intercalation driving force, allowing only a minimal amount of anthracene to enter the organic montmorillonite interlayers. These sparsely dispersed anthracene molecules in the interlayer caused the montmorillonite sheets to stack disorderly along the *c*-axis. As the concentration of intercalated anthracene increased, the anthracene molecules distributed more uniformly within the montmorillonite layers. This arrangement restored the ordered stacking of montmorillonite sheets, leading to the appearance of distinct (001) crystal plane diffraction peaks in the composite's XRD pattern. Furthermore, these diffraction peaks shifted to lower angles with increasing anthracene concentration, indicating a gradual expansion of the interlayer spacing in the composite. This confirmed that anthracene molecules successfully entered the organic montmorillonite layers. Additionally, the diffraction peaks of anthracene crystals began to appear in the composite's XRD pattern as the anthracene concentration increased. This is likely because, while some anthracene molecules entered the organic montmorillonite interlayers, others were adsorbed onto the surface of the organic montmorillonite.

To understand the chemical structure of the composites, FTIR spectroscopy was performed on anthracene, modified montmorillonite, and the composites.

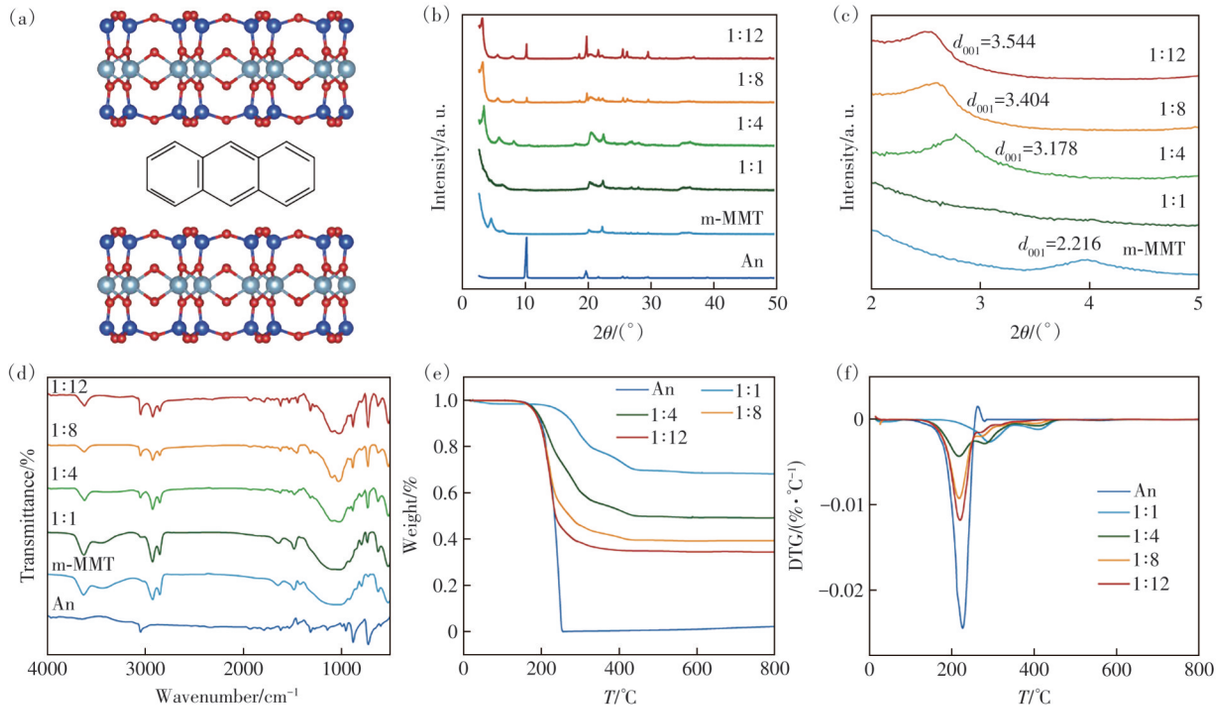

Fig.1　(a) Schematic illustration of the layered structure of montmorillonite and the intercalation configuration of the anthracene (An)-modified montmorillonite composite (anthracene molecular structure shown in the center). (b) X-ray diffraction (XRD) patterns of An, modified montmorillonite (m-MMT), and the composites labeled as 1∶1, 1∶4, 1∶8, and 1∶12. (c) Enlarged XRD patterns in the 2θ range of 2°–5°, showing the (001) basal spacing (d_{001}): 2.216 nm (m-MMT), 3.178 nm (1∶4), 3.404 nm (1∶8), and 3.544 nm (1∶12). FTIR spectra and thermal stability analyses of An, m-MMT and the composites (1∶1, 1∶4, 1∶8 and 1∶12): (d) FTIR spectra (An, m-MMT, 1∶1, 1∶4, 1∶8, 1∶12). (e) TG curves. (f) DTG curves

The results are shown in Fig. 1(d). It represents anthracene, modified montmorillonite, and the composites from the bottom to top. Analyzing the spectrum of anthracene, the absorption peak at 467 cm^{-1} is attributed to the out-of-plane bending vibration of the entire anthracene molecule driven by the bending vibration of the aromatic C═C bonds. The peaks at 725 cm^{-1}, 879 cm^{-1}, and 954 cm^{-1} are caused by the out-of-plane bending vibrations of the C—H bonds in the structure. Additionally, the absorption peak at 3 046 cm^{-1} is a characteristic peak of anthracene, with a relatively complex origin. In the spectrum of organic m-MMT, the weak absorption bands at 3 437 cm^{-1} and 1 645 cm^{-1} correspond to the stretching and bending vibrations of the O—H bonds of small amounts of water in the montmorillonite interlayers. The absorption bands at 3 631 cm^{-1} and 796 cm^{-1} are characteristic peaks of the Al(Mg)—OH bonds, while the bands at 521 cm^{-1} and 463 cm^{-1} can be attributed to the stretching and bending vibrations of Si—O bonds, respectively. Furthermore, the sharp absorption peaks at 2 854 cm^{-1}, 2 925 cm^{-1}, and 1 485 cm^{-1} are associated with the symmetric stretching, asymmetric stretching, and bending vibrations of the C—H bonds in the CTAB molecular structure. These results indicate that the CTAB modifier molecules successfully entered the montmorillonite interlayers. Examining the spectra of the composites, their shapes are generally similar to that of organic montmorillonite. As the intercalation concentration increased, the characteristic peaks of anthracene at 725 cm^{-1}, 879 cm^{-1}, and 3 046 cm^{-1} gradually appeared in the composite spectra. Additionally, the water characteristic peaks at 3 437 cm^{-1} and 1 645 cm^{-1} almost disappeared, indicating that anthracene successfully intercalated into the organic montmorillonite layers. This resulted in a more hydrophobic interlayer environment, effectively eliminating the presence of water molecules.

To investigate the thermal stability of the composites, thermogravimetric (TG) analysis was conducted,

and the results are shown in Fig. 1(f). From the TG and DTG curves, it can be observed that pure anthracene begins to decompose at around 84 ℃. As the temperature rises, the decomposition rate increases rapidly, reaching its peak at 226 ℃. By 250 ℃, the remaining mass of anthracene is nearly zero, indicating that the anthracene crystals are completely decomposed at this point. Examining the thermal weight loss curves of the composites and comparing them with the curve of raw montmorillonite presented, it is evident that the composites exhibit almost no mass loss below 100 ℃. This indirectly confirms the absence of water molecules within the montmorillonite interlayers, consistent with the hydrophobic environment identified in the FTIR results. For the composite with an intercalation ratio of 1∶1, significant mass loss begins at approximately 166 ℃. For composites with intercalation ratios of 1∶4, 1∶8, and 1∶12, the temperatures at which mass loss starts are 103 ℃, 98 ℃, and 93 ℃ respectively. This suggests that the montmorillonite layers can provide some degree of thermal protection for the anthracene molecules. Specific data are detailed in Tab. 1.

Tab. 1 Onset and end temperatures of weight loss for the samples

Sample	Start/℃	End/℃
An	84	240
1∶1	166	468
1∶4	103	477
1∶8	98	452
1∶12	93	430

Fig. 2(a) and 2(b) present the SEM images of the raw clay mineral and the composites. They correspond to raw montmorillonite and the intercalated montmorillonite material, respectively. During the preparation of the composites, the clay mineral underwent a stirring exfoliation process in water, allowing water molecules to expand the interlayer spacing of the clay. Notably, the layered structure of the clay mineral remained intact. Fig. 2(c)-2(f) show the SEM image of the anthracene/organic montmorillonite composite. Compared to raw montmorillonite, the microstructure of the montmorillonite has undergone

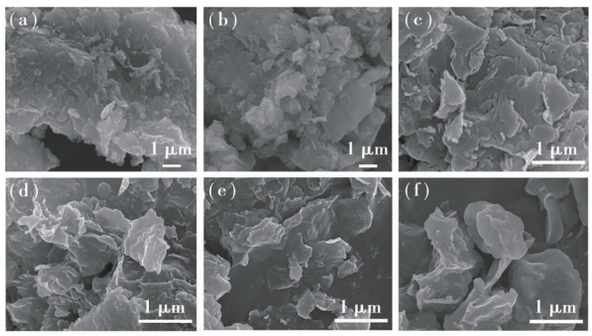

Fig.2 SEM images of the raw clay mineral and the corresponding composites. (a)Pristine montmorillonite (MMT). (b)Intercalated montmorillonite. (c)-(f) SEM images of different anthracene/organically modified montmorillonite(An/m-MMT) composites, corresponding to the samples labeled as 1∶1, 1∶4, 1∶8, and 1∶12. Scale bar: 1 μm

significant changes. The montmorillonite layers remain intact but exhibit greatly enhanced dispersion. The mineral layers are loosely stacked, and the edges of the layers are curled and twisted, contrasting sharply with the compact structure of the raw montmorillonite. This transformation is attributed to the organic modification process, where CTAB enters the montmorillonite interlayers. With its long alkyl tail chains, CTAB occupies significant space within the interlayers, increasing the interlayer spacing of montmorillonite. This observation is consistent with the XRD results: the d_{001} spacing of raw montmorillonite is 1.523 nm, while that of organic montmorillonite is 2.216 nm. After anthracene intercalates into the organic montmorillonite layers, the interlayers are filled with hydrophobic organic molecules. This weakens the electrostatic attraction between the negatively charged montmorillonite sheets and the interlayer cations, leading to the formation of the loosely stacked layered structure.

3.2 Fluorescence Performance of Anthracene/Organic Montmorillonite Composites

In this study, anthracene was selected as the organic luminescent small molecule. As shown in Fig. 3(a), anthracene features a rigid fused-ring framework, and it emits bright fluorescence under 365 nm UV excitation (Fig. 3(b)). Fig. 3(c) shows the fluorescence excitation and emission spectra of anthracene used in this experiment. Observing the

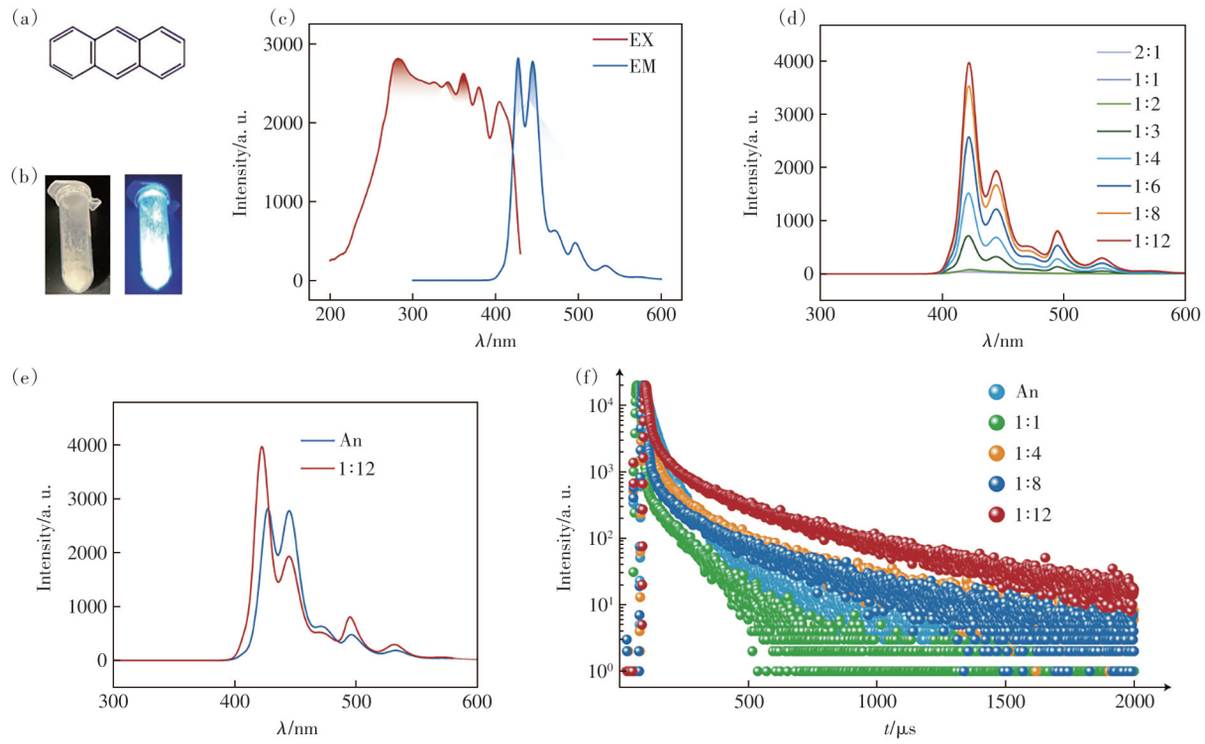

Fig.3　Photoluminescence properties of anthracene (An) and An-intercalated composites. (a) Molecular structure of anthracene (An). (b) Photographs of An under daylight (left) and 365 nm UV irradiation (right). (c) Excitation (EX) and emission (EM) spectra of An. (d) Steady-state fluorescence spectra of the An-intercalated composites with increasing An loading from 2∶1 to 1∶12 (from bottom to top). (e) Fluorescence spectra of pristine An and the 1∶12 composite. (f) Time-resolved fluorescence decay curves of An and selected composites (1∶1, 1∶4, 1∶8, and 1∶12)

excitation spectrum (red curve), multiple peaks form a broad band within the range of 200–420 nm, indicating that anthracene has strong energy absorption capabilities across a wide range in the ultraviolet region. The optimal excitation wavelength is 282 nm. Using 282 nm ultraviolet light as the excitation wavelength, the emission spectrum of anthracene (blue curve) was obtained. The emission spectrum reveals two strong fluorescence peaks at 427 nm and 445 nm, both in the blue light region. Additionally, three weaker fluorescence emission peaks appear at 471 nm, 496 nm, and 533 nm.

To investigate the luminescence behavior of the composites, their fluorescence spectra were measured with 282 nm as the excitation wavelength, and the results are shown in Fig. 3(d). the fluorescence emission peaks of the composites differ significantly in shape compared to pure anthracene. In pure anthracene, the intensities of the two emission peaks at 427 nm and 445 nm are nearly identical. However, after combining with organic montmorillonite, the long-wavelength emission peak of the composite becomes significantly weaker than the short-wavelength emission peak. This phenomenon may result from the interaction between anthracene and the interlayer CTAB or differences in the arrangement of anthracene molecules. In the charged interlayer domain of organic montmorillonite, anthracene molecules are dispersed in a specific orientation, whereas in pure anthracene, the molecules are tightly packed. From the fluorescence spectra of the composites, it is evident that as the amount of intercalated anthracene increases, the fluorescence intensity of the composites also increases. When the intercalation concentration reaches 1∶12, the fluorescence intensity of the composites significantly exceeds that of pure anthracene (Fig. 3(e)). Under ultraviolet light, the luminescence of the composites and pure anthracene aligns with the fluorescence spectra results. As the intercalation concentration increases, the fluorescence brightness of the composites is significantly enhanced, transitioning from dim blue at

low concentrations to bright blue at high concentrations. It is attributed to the electric field effect within the interlayer domain, which causes anthracene molecules to be uniformly dispersed in the interlayer, effectively suppressing fluorescence quenching caused by aggregation or stacking of anthracene molecules.

Fluorescence lifetime is an important parameter reflecting the stability of luminescent materials. The luminescence decay curves of the composites were measured under an excitation wavelength of 282 nm and an emission wavelength of 427 nm, as shown in Fig. 3(f). The lifetime curves were fitted using a three-exponential function described by Eq. (1)[32]:

$$I(t) = I_0 + A_1\exp\left(-\frac{t}{\tau_1}\right) + A_2\exp\left(-\frac{t}{\tau_2}\right) + A_3\exp\left(-\frac{t}{\tau_3}\right), \tag{1}$$

the luminescence lifetime curve is the curve showing the decay of the material's luminescence intensity over time. In the formula, I_0 and $I(t)$ represent the initial luminescence intensity and the luminescence intensity at time t, respectively. A_i is a constant, and τ_i is the decay time of the exponential component. After fitting the lifetime curve, the values of A_i and τ_i for each material can be obtained. The fluorescence lifetime can be calculated using Eq. (2):

$$\tau^* = \frac{A_1\tau_1^2 + A_2\tau_2^2 + A_3\tau_3^2}{A_1\tau_1 + A_2\tau_2 + A_3\tau_3}, \tag{2}$$

the calculation shows that the fluorescence lifetime of pure anthracene is 48.77 μs, while the fluorescence lifetime of the composites with intercalated anthracene concentrations of 1∶1, 1∶4, 1∶8, and 1∶12 is 98.73 μs, 102.76 μs, 136.22 μs, and 107.74 μs, respectively. The fluorescent lifetime of the composites is significantly longer compared to pure anthracene. It is speculated that this phenomenon may be due to the more stable environment provided by the montmorillonite layers for anthracene, which reduces non-radiative energy loss caused by molecular vibrations, thereby improving the luminescent performance.

3.3 Pressure-dependent Spectroscopy

Under external pressure, most organic luminescent materials exhibit a gradual red shift accompanied by fluorescence quenching in their emission spectra. Using this characteristic, such materials can be employed in pressure sensing and optical display devices. To explore the changes in luminescence intensity and color of composite luminescent materials under varying external pressures, the anthracene/organic montmorillonite composite synthesized in this study was tested for such optical properties. In this experiment, the pressure-dependent spectroscopy of the samples was tested using a Diamond Anvil Cell (DAC) device, and its core components are shown in Fig. 4(a). The DAC consists of a pair of diamond anvils, with the test material placed in the sample chamber between the two anvils, where pressure is applied in the vertical direction. Diamonds are highly durable and can withstand extreme external pressures. Furthermore, diamonds have excellent transparency to a wide range of electromagnetic waves, including X-rays, ultraviolet light, visible light, and infrared light. Thus, the DAC device allows for the acquisition of spectroscopic data of the sample under high pressure.

First, the pressure-dependent spectrum of the composite material was measured, and the results are shown in Fig. 4(b) and 4(c). As the external pressure increased from 101.32 kPa(1 atm), the fluorescence spectrum of anthracene changed in two stages: As the external pressure increased from 101.32 kPa to 1.60 GPa, the intensity of both characteristic fluorescence peaks of anthracene decreased, and the positions of the peaks exhibited a red shift. The two emission peaks gradually merged into a new fluorescence emission peak (Fig. 4(b), stage 1). As the external pressure increased further from 1.60 GPa to 10.1 GPa, the intensity of the merged fluorescence emission peak gradually decreased, and its position shifted further to the red (Fig. 4(c), stage 2). In the two-stage variation of the fluorescence spectrum with pressure, the changes in the mixed fluorescence emission peak's intensity and position in stage 2 are more easily observed, and the pattern of change is clearer. Therefore, the following discussion will focus on the second-stage pressure-dependent spectroscopy of the anthracene/organic montmorillonite

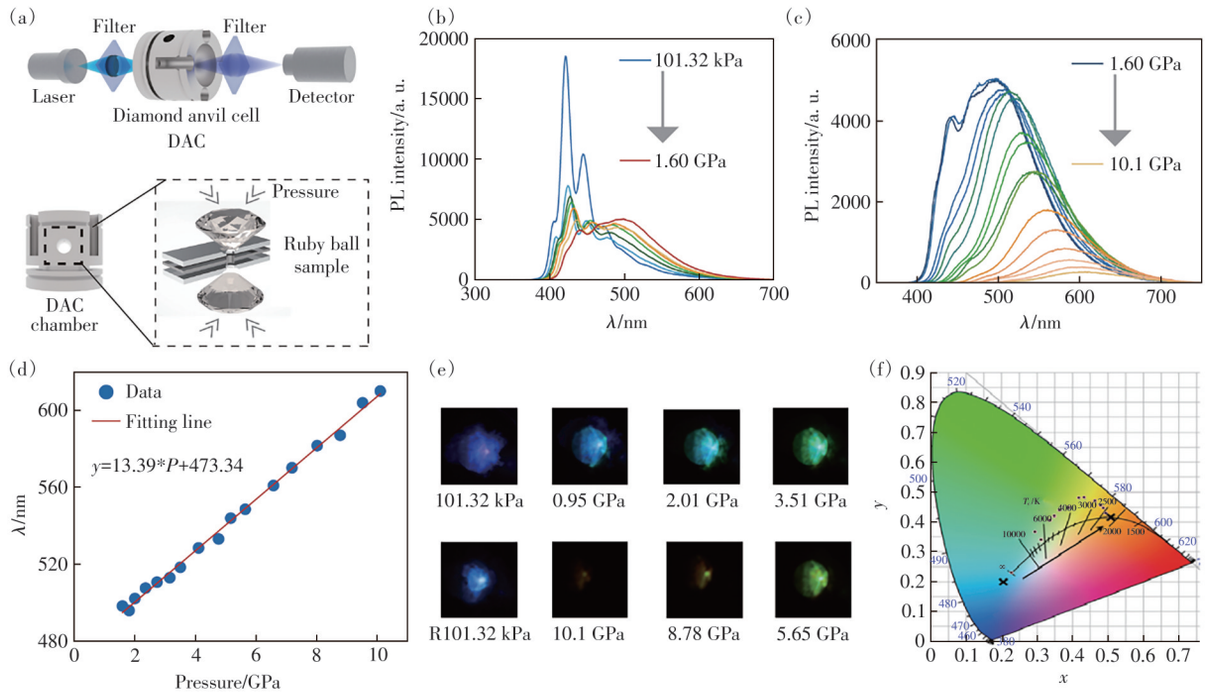

Fig.4　*In situ* high-pressure photoluminescence of the 1∶12 composite measured in a diamond anvil cell (DAC). (a) Schematic illustration of the experimental setup for DAC-based photoluminescence (PL) measurements, where the sample and a ruby chip were loaded into the DAC chamber for pressure calibration. (b), (c) Pressure-dependent PL spectra of the 1∶12 composite recorded in two pressure windows: from ambient pressure (101.32 KPa) to 1.60 GPa (b), and from 1.60 GPa to 10.1 GPa (c), arrows indicate increasing pressure. (d) Evolution of the PL peak wavelength as a function of applied pressure, together with a linear fit to the experimental data. (e) Digital photographs of the composite under 365 nm UV irradiation at representative pressures during compression and release (R), showing a distinct pressure-induced color change. (f) Corresponding CIE 1931 chromaticity coordinates derived from the PL spectra, illustrating the pressure-tunable emission color trajectory

composite material. The intensity and wavelength of the fluorescence emission peaks at different pressures in stage 2 were fitted, as shown in Fig. 4(d). The wavelength of the fluorescence emission peaks in the composite material shows a good linear relationship with the external pressure Eq. (3):

$$y = A + Bx, \tag{3}$$

the linear relationship between the fluorescence emission peak wavelength (λ) and the applied pressure (P) is described by the equation $\lambda = A + B \cdot P$. From the fitting, the intercept A=473.3 nm, the slope B=13.4 nm/GPa, and the goodness of fit to Eq. (3) is R^2=0.996. This indicates that within the pressure range of 1.60 GPa to 10.1 GPa, as the external pressure increases, the wavelength of the composite material's fluorescence emission peak undergoes a regular red shift. From the fluorescence photographs of the composite material under different pressures (Fig. 4(e)), it is evident that the fluorescence color of anthracene underwent significant changes, transitioning from blue-violet to cyan-blue, green, and yellow, with a corresponding decrease in fluorescence brightness. Corresponding CIE 1931 chromaticity coordinates derived from the PL spectra are also shown in Fig. 4(f).

From the above analysis, it is clear that within the tested pressure range of 1.60 GPa to 10.1 GPa, the wavelength of the composite material's fluorescence emission peak can respond sensitively to external pressure, with this parameter serving as a signal for measuring environmental pressure. This characteristic gives the anthracene/organic montmorillonite composite luminescent material great potential for applications in pressure sensing. Furthermore, during the pressure release process, as the pressure decreases, the intensity of the fluorescence emission peak recovers while its position blue-shifts. When the pressure returns to 101.32 kPa, the emission

peak's position nearly returns to its initial state.

4 Conclusion

This work demonstrates an interlayer-confinement route to translate the pressure sensitivity of an organic luminophore into a readable and quantifiable optical signal. Anthracene (An) was successfully intercalated into CTAB-modified montmorillonite, evidenced by the systematic expansion of the (001) basal spacing from 2.216 nm (m-MMT) to 3.544 nm (1∶12), confirming effective gallery confinement and dispersion. Steady-state photoluminescence shows that the emission intensity increases with An loading and becomes higher than pristine An at the highest intercalation level, while time-resolved decay measurements indicate a prolonged emission lifetime after confinement. Under diamond-anvil-cell compression, the 1∶12 composite exhibits pronounced piezochromism: the emission evolves in two stages and, in the high-pressure regime (1.60–10.1 GPa), the merged emission peak red-shifts in a highly linear manner with pressure (13.4 nm/GPa, R^2=0.996), accompanied by a visible color transition from bluish-violet toward yellow; partial recovery is observed upon decompression. Overall, these results indicate that interlayer confinement can both suppress solid-state quenching and enable quantitative optical manometry, providing a practical materials strategy for visualization-enabled pressure sensing in extreme environments.

Response Letter is available for this paper at: http://cjl.lightpublishing.cn/thesisDetails#10.37188/CJL.20260002

References:

[1] MCCONNELL A J, WOOD C S, NEELAKANDAN P P, *et al*. Stimuli-responsive metal-ligand assemblies [J]. *Chem. Rev.*, 2015, 115(15): 7729-7793.

[2] THEATO P, SUMERLIN B S, O'REILLY R K, *et al*. Stimuli responsive materials [J]. *Chem. Soc. Rev.*, 2013, 42(17): 7055-7056.

[3] FU Z Y, WANG K, ZOU B. Recent advances in organic pressure-responsive luminescent materials [J]. *Chin. Chem. Lett.*, 2019, 30(11): 1883-1894.

[4] XIE M, CHEN X R, WU K, *et al*. Pressure-induced phosphorescence enhancement and piezochromism of a carbazole-based cyclic trinuclear Cu(I) complex [J]. *Chem. Sci.*, 2021, 12(12): 4425-4431.

[5] SU K, MEI L F, GUO Q F, *et al*. Multi-mode optical manometry based on $Li_4SrCa(SiO_4)_2$: Eu^{2+} phosphors [J]. *Adv. Funct. Mater.*, 2023, 33(49): 2305359.

[6] SZYMCZAK M, SU K, MEI L F, *et al*. Investigating the potential of Cr^{3+}-doped pyroxene for highly sensitive optical pressure sensing [J]. *ACS Appl. Mater. Interfaces*, 2024, 16(44): 60491-60500.

[7] DONG Y J, XU B, ZHANG J B, *et al*. Piezochromic luminescence based on the molecular aggregation of 9, 10-Bis((*E*)-2-(pyrid-2-yl)vinyl)anthracene [J]. *Angew. Chem.*, 2012, 124(43): 10940-10943.

[8] ZHENG T, RUNOWSKI M, MARTÍN I R, *et al*. Mechanoluminescence and photoluminescence heterojunction for superior multimode sensing platform of friction, force, pressure, and temperature in fibers and 3D-printed polymers [J]. *Adv. Mater.*, 2023, 35(40): 2304140.

[9] VIRENDER, CHAUHAN A, KUMAR A, *et al*. Photonic properties and applications of multi-functional organo-lanthanide complexes: recent advances [J]. *J. Rare Earths*, 2024, 42(1): 16-27.

[10] YANG X Q, DAI Y X, LIU H C, *et al*. Antagonistic effects of distance and overlap toward anomalous pressure-induced blueshift of π-π excimer fluorescence in 9-(2, 2-diphenylvinyl) anthracene crystals [J]. *J. Am. Chem. Soc.*, 2025, 147(6): 5300-5309.

[11] YU X H, FANG Y Y, SUN X N, *et al*. Pressure-tuning localized excitons toward enhanced emission, photocurrent enhancement and piezochromism in unconventional ACI-type 2D hybrid perovskites [J]. *Angew. Chem. Int. Ed.*, 2024, 63(46): e202412756.

[12] WANG L, YE K Q, ZHANG H Y. Organic materials with hydrostatic pressure induced mechanochromic properties [J].

Chin. Chem. Lett., 2016, 27(8): 1367-1375.

[13] QI G Y, WANG K, LI X D, *et al.* High pressure behavior of hydrogen storage material guanidinium borohydride [J]. *J. Phys. Chem.* C, 2016, 120(25): 13414-13420.

[14] ZHANG G, MEI L F, DING J J, *et al.* Recent progress on lanthanide complexes/clay minerals hybrid luminescent materials [J]. *J. Rare Earths*, 2022, 40(9): 1360-1370.

[15] TAN K M, ZENG Y, SU L, *et al.* Molecular dual-rotators with large consecutive emission chromism for visualized and high-pressure sensing [J]. *ACS Omega*, 2018, 3(1): 717-723.

[16] GAO S S, WANG S Q, WU J Y, *et al.* Regulation and application of organic luminescence from low-dimensional organic-inorganic hybrid metal halides [J]. *J. Mater. Chem.* C, 2023, 11(48): 16890-16911.

[17] QI G Y, WANG K, XIAO G J, *et al.* High pressure, a protocol to identify the weak dihydrogen bonds: experimental evidence of C—H···H—B interaction [J]. *Sci. China Chem.*, 2018, 61(3): 276-280.

[18] DONG Y J, ZHANG J B, TAN X, *et al.* Multi-stimuli responsive fluorescence switching: the reversible piezochromism and protonation effect of a divinylanthracene derivative [J]. *J. Mater. Chem.* C, 2013, 1(45): 7554-7559.

[19] BLOCK S, WEIR C E, PIERMARINI G J. Polymorphism in benzene, naphthalene, and anthracene at high pressure [J]. *Science*, 1970, 169(3945): 586-587.

[20] VAN DAMME J, DU PREZ F. Anthracene-containing polymers toward high-end applications [J]. *Prog. Polym. Sci.*, 2018, 82: 92-119.

[21] LIM H, WOO S J, HA Y H, *et al.* Breaking the efficiency limit of deep-blue fluorescent oleds based on anthracene derivatives [J]. *Adv. Mater.*, 2022, 34(1): 2100161.

[22] GARCI A, BELDJOUDI Y, KODAIMATI M S, *et al.* Mechanical-bond-induced exciplex fluorescence in an anthracene-based homo[2]catenane [J]. *J. Am. Chem. Soc.*, 2020, 142(17): 7956-7967.

[23] TSYUPKA D V, PODKOLODNAYA Y A, KHUDINA E A, *et al.* Anthracycline antibiotics detection using turn-off luminescent nanosensors [J]. *TrAC Trends Anal. Chem.*, 2024, 177: 117774.

[24] HU Q, DUAN C, WU J J, *et al.* Colorimetric and ratiometric chemosensor for visual detection of gaseous phosgene based on anthracene carboxyimide membrane [J]. *Anal. Chem.*, 2018, 90(14): 8686-8691.

[25] WAN H, YAN A L, XIONG H, *et al.* Montmorillonite: a structural evolution from bulk through unilaminar nanolayers to nanotubes [J]. *Appl. Clay Sci.*, 2020, 194: 105695.

[26] FERREIRA A U C, POLI A L, GESSNER F, *et al.* Interaction of auramine o with montmorillonite clays [J]. *J. Lumin.*, 2013, 136: 63-67.

[27] ZHAI Y C, SHEN F Z, ZHANG X T, *et al.* Synthesis of green emissive carbon dots@montmorillonite composites and their application for fabrication of light-emitting diodes and latent fingerprints markers [J]. *J. Colloid Interface Sci.*, 2019, 554: 344-352.

[28] WU L M, BAO X Y, ZHONG H Y, *et al.* Preparation of a novel clay/dye composite and its application in contaminant detection [J]. *Clays Clay Miner.*, 2019, 67(3): 244-251.

[29] HALIM N A, IBRAHIM Z A, AHMAD A B. Intercalation of water and guest molecules within Ca^{2+}-montmorillonite [J]. *J. Therm. Anal. Calorim.*, 2010, 102(3): 983-988.

[30] TEEPAKAKORN A P, BUREEKAEW S, OGAWA M. Adsorption-induced dye stability of cationic dyes on clay nanosheets [J]. *Langmuir*, 2018, 34(46): 14069-14075.

[31] TANGARAJ V, JANOT J M, JABER M, *et al.* Adsorption and photophysical properties of fluorescent dyes over montmorillonite and saponite modified by surfactant [J]. *Chemosphere*, 2017, 184: 1355-1361.

[32] CHANG M F, LI L, HU H Y, *et al.* Using fractional intensities of time-resolved fluorescence to sensitively quantify NADH/NAD^+ with genetically encoded fluorescent biosensors [J]. *Sci. Rep.*, 2017, 7(1): 4209.

张光晴(1999–),男,河南焦作人,硕士研究生,2021年于青海大学获得学士学位,主要从事无机荧光粉的合成以及高压下材料光学性能的研究。
E-mail: zgqawm@sina.com

梅乐夫(1978–),男,湖南常德人,博士,教授,博士生导师,2007年于清华大学获得博士学位,主要从事稀土发光与光电功能材料的研究。
E-mail: mlf@cugb.edu.cn